Environmental Science Nano

Graphene Oxide Membranes on a Hierarchical Elemental Carbon-based Support

Journal:	*Environmental Science: Nano*
Manuscript ID	EN-ART-10-2019-001136.R2
Article Type:	Paper

The water crisis is one of the greatest challenges of our time and is exacerbated by anthropogenic phenomena, such as climate change and increased water demand, that also undermine access to clean water. Although groundwater plays a pivotal role in the water supply, new technological advances are needed to supply water in a more sustainable manner. One of these technologies is wastewater reclamation, in which wastewater is treated to a level that can be reused, thus avoiding the withdrawal of new freshwater from the natural cycles. Innovation in wastewater reclamation can rely on the use of new nanomaterials with more effective filtration. This paper through the synthesis of new hierarchical carbon membranes tries to support this research effort.

Graphene Oxide Membranes on a Hierarchical Elemental Carbon-based Support

*Carlo Alberto Amadei[1], Paula Arribas[2], Luis Cruzado,[3] Chad D. Vecitis[1]**

[1]John A. Paulson School of Engineering and Applied Sciences, Harvard University, Cambridge, MA 02138, USA
[2]Department of Structure of Matter, Thermal Physics and Electronics, Faculty of Physics, Complutense University of Madrid, Madrid 28040, Spain
[3]Water Quality Improvement Center, United States Bureau of Reclamation, Yuma, AZ 85364, USA

*corresponding author: E-mail vecitis@seas.harvard.edu (Chad D. Vecitis)

KEYWORDS: graphene, carbon, chemical resistant, thermal resistant, wastewater.

ABSTRACT

Carbon-based materials have been used in water engineering to provide more effective and efficient methods to deliver clean water. Recent research efforts have focused on the implementation of nanoarchitectured carbon molecular sieves in membranes. In this study, a hierarchical carbon membrane (HCM), fully-constituted by elemental carbon structures from the carbon fiber mechanical support to the graphene oxide selective layer, was fabricated. The assembled HCM were characterized by a combination of surface science tools, capillary flow porometry, thermogravimetric analysis, and membrane performance evaluation. The HCM were resistant to harsh cleaning by hypochlorite solutions and annealing cycles (similar to ceramic membranes). The HCM permeability and rejection performance were evaluated in a cross-flow setup and indicate the membrane operates in the nanofiltration regime, with 85% rejection of sulfate ions and 1.3 LMH-bar permeability. In summary, the results here support the emerging research direction of hierarchal fully elemental carbon membrane materials to enhance the membrane technology toolbox for sustainable water resource reuse and wastewater reclamation.

1. INTRODUCTION

Carbon materials have been utilized to solve numerous technical challenges due to their tunable chemo-morphological properties.[1],[2] The emergence of carbon nanomaterials, together with the discovery of graphene,[3] has further enhanced the potential range of carbon applications.[4],[5],[6] Nanotechnology allows for a near infinite number of chemical-morphological combinations with only a few elements and rationally tune those properties for specific applications, yielding the implementation of carbon nanoarchitectures in a vast variety of engineering fields ranging from environmental [7],[8] to aerospace applications.[9]

In water engineering applications alone, elemental carbon nanomaterials have been applied in many different forms such as carbon nanotubes (CNT), graphene oxide (GO), and activated carbons in order to adsorb and/or sieve aqueous contaminants.[10],[11],[12],[13] Although these nanocarbon forms differ greatly from one another in terms of chemical functionalization and physical morphology, they all tend to display a high surface specific area tunable properties, and chemical/thermal stability.[14],[15] These shared characteristics make elemental carbon-based membranes a potential alternative to more common ceramic and polymeric membranes. On the one hand, ceramic membranes exhibit advantages of thermal/chemical stability and a straightforward cleaning processes.[16] On the other hand, polymeric membranes feature advantages of minimal thickness, low cost, and easily tunable properties, which allows them to excel in industrial and municipal applications such as nanofiltration (NF).[17] (Note, that in this paper, we refer to NF regime following the IUPAC definition: a membrane-based separation process in which particles and dissolved molecules smaller than about 2 nm are rejected.[18])

A chemically and thermally resistant membrane resilient to harsh cleaning (typical of ceramic membranes) and able to operate in the nanofiltration regime (dominated by polymer membranes) has potential for a range of water treatment applications. In particular, advanced wastewater treatment (AWWT) applications that aim to reclaim wastewater for reuse purposes such as urban, agricultural, environmental, and potable uses. Although the overall AWWT process varies depending on feed quality and effluent requirements, membranes processes are routinely utilized to remove ions and organic molecules and meet strict environmental standards. Currently, AWWT membrane processes are dominated by polyamide polymeric membranes, which are subject to fouling and cleaning issues due to their low chemical resistance.[19] Membrane fouling leads to increased treatment plant operational and maintenance (O&M) cost due to cleaning chemical cost and increased plant downtime. For

instance, a two-fold more expensive chlorine-resistant nanofiltration membrane will yield savings in the overall plant O&M due to the reduction of chemicals use and downtime.[20] Previous studies have investigated using a protective layer to enhance the selectivity or the chemical stability of the membranes. For example, GO embedded in reverse osmosis membranes drastically improved the chlorine resistance due to prevention of polyamide chlorination.[21] However, the chemical resistance was limited to the selective layer, as the polymer-based substrate was subject to degradation when oxidizing agents permeate the membranes.[22],[23]

Previous studies have investigated chemically-reduced GO NF selective layers to enhance mechanical stability and rejection performance. For instance, Han *et al.* deposited a ~100 nm thick NaOH-reduced GO layer onto a PVDF membrane that was able to completely reject (>99%) of organic dyes.[24] The complete rejection of organic dyes could also be obtained using a hydrazine-reduced GO selective layer.[25] Diamine and cation cross-linked GO selective layers been observed to achieve high NF rejection of multivalent ions.[26],[27] In all previous studies highlighted here, the GO layer was cast onto a polymer membrane substrate and the poor chemical resistance of the substrate will result in membrane deterioration when subject to harsh chemical cleaning. Moreover, polymer-based membranes will also limit the membrane operating temperature as well as the permeating fluid properties. Ceramic substrates for GO selective layers are a possible solution to the polymer stability disadvantages,[28] however, this would significantly increase the membrane capital cost. Thus, here we will investigate the use of hierarchal elemental carbon substrates as both a stable and low-cost alternative to polymer and ceramic substrates.

Motivated by the aim to develop cost-effective AWWT solutions, we hypothesized that a hierarchal carbon membrane (HCM) operating in the NF regime could be assembled with the exclusive use of elemental carbon materials with no polymers or ceramics, i.e. the elemental composition of all materials is >75% carbon and the monomer repeating units of a polymer/ceramic have been replaced with elemental carbon architectures. This research takes inspiration from carbon molecular sieves (CMS) obtained by the carbonization of a polymer matrix which are used for energy storage and gas separation applications.[29],[30] The CMS hierarchical structure is then a consequence of the pores dimensions, a result of the carbonization process. In contrast, we decided to pursue an alternative approach where the hierarchy is dictated by the dimension of the individual elemental carbon nanoarchitectures deposited in a sequential manner. Thus here, the complete HCM was fabricated via a 3D printed custom-made vacuum filtration system by sequential deposition of a micrometer-diameter

carbon fiber (CF) substrate support, a nanometer-diameter carbon nanotube (CNT) intermediate layer, and an atomically-thin GO selective layer.

The research also builds upon previous investigations by Goh *et al.* in which only the selective layer was constituted of carbon architectures[22] and by Kim in which a free-standing carbon membrane was manufactured to separate dyes.[31] In this study, the rejections of ions, rather than traditionally-used organic molecules (e.g., dyes), was examined to circumvent any experimental artifacts as a result of the high aromatic adsorption capacity to elemental carbon materials.[32] Thus by using ions, the predominant rejection/removal mechanism will be related to physical size exclusion and not adsorption. Moreover, this investigation is based on external pressure driven filtration experiments (4-10 bar similar to practical real-world applications) in which the membranes are subject to significantly higher mechanical stress as compared to diffusive permeation experiments.

Here, we fabricated the HCM by sequential vacuum filtration of a CF substrate, a CNT intermediate support layer, and finally a GO selective layer. The HCM were characterized SEM, XPS, capillary flow porometry, thermogravimetric analysis, and membrane performance. The HCM potential for AWWT is focused on two main performance measures: i) the capability of the membranes to reject ions in a cross-flow apparatus (typical of municipal applications) before and after extreme cleaning processes; and ii) the chemical and thermal resistance of the membranes challenged by permeation of oxidizing agents and annealing cycles.

2. EXPERIMENTAL

2.1 Chemicals and Materials

The Spectracarb 2050-1050 GDL CF paper was purchased from *Engineering Fiber Technology*. C-grade multiwalled nanotubes (CNT) with >95% purity were purchased from *NanoTechLabs (*Yadkinville, NC*)*. Graphene oxide (GO) aqueous solutions (~4 mg/mL) were purchased from *Graphenea* (Cambridge, MA*)*. Sodium sulfate (Na_2SO_4, ≥99%), sodium chloride (NaCl, ≥97%), and sodium hydroxide (NaOH, ≥97%) were purchased from *Sigma-Aldrich*, sodium hypochlorite (NaClO, 8%) and isopropyl alcohol (IPA, 99%) were purchased from *VWR chemicals,* and 5% wt. Nafion solution was purchased from *Fuel Cell Earth*

(Woburn, MA). Commercially available NF270 polyamide flat sheet membrane was purchased from *Sterlitech*.

2.2 Membrane Fabrication

A flowchart in Figure S1 in the Supplementary Information (SI) summarizes the overall fabrication process. First, a CNT solution was prepared by mixing 30 mg of CNT with 60 mL of IPA and 0.2 mL of Nafion solution (5 wt.%). This solution was dispersed by probe-sonication (Sonifier S-450D with high gain horn; *Branson Ultrasonics Corp.)* at 50% of the maximum amplitude (100 W) for 3 min, and subsequently, bath sonicated for 4 min in a *Branson* sonicator (V = 1.9 L, maximal power = 80 W, and f = 20 kHz). The use of Nafion to increase the dispersion was observed in previous studies.[33] Also, note that without the use of Nafion only a poor colloidal stability can be achieved. The obtained CNT solution was vacuum filtered onto a CF paper (1st layer, substrate of the HCM) using a custom 3D printed filtration system (see Figure S2 in the SI). Another solution containing GO and CNT was prepared in the same manner as the first CNT solution but also included 0.15 mL of GO solution (~4 mg/mL) added prior to the bath sonication step. This GO-CNT solution was then vacuum filtrated onto the CF-CNT composite substrate, constituting a transition layer between the intermediate CNT support layer (2nd layer) and the final GO selective layer (3rd layer). From our empirical evidence, this mixed layer increased membrane stability. Then, a 0.2 mL GO solution (~4 mg/mL) was diluted with 80 mL of DI water and bath sonicated for 1 min. The final GO solution was then filtered onto the GO-CNT transition layer, constituting the selective layer of the HCM. Finally, the HCM was thermally reduced at 150 °C for 20 min in an inert atmosphere (i.e. N_2) with the use of a *Thermolyne* 21100 tube furnace, in order to increase membrane stability. Once the HCM was prepared, it was cut with a razor blade in a rectangular shape (8 x 4 cm^2) and placed into the filtration device for testing. HCM were initially tested for integrity by permeating through DI at 5 bar of applied pressure and only those passing the test (i.e., permeability < 30 LMH-bar (i.e., L $m^{-2}h^{-1}bar^{-1}$) indicating overall structural integrity) were used in subsequent experiments. The value of 30 LMH-bar was chosen because that was the permeability of the CF-CNT layer without GO.

The fabrication method is based on vacuum filtration (VF) as it is the most common method to fabricate GO membranes and there is an extensive literature on its optimization.[34]

2.3 HCM Characterization

Scanning Electron Microscopy (SEM). The morphology and structure of the HCM were characterized using a *Zeiss ULTRA* Field Emission Scanning Electron Microscope with an In-lens secondary electron detector. The working distance was 3-4 mm, and the acceleration voltage was 5 kV. The statistical SEM image analysis of the HCM layers was completed using *ImageJ* software to calculate pore size and the dimension of the carbon architectures.

X-ray Photoelectron Spectroscopy (XPS). HCM surface chemistry was analyzed by a *Thermo Scientific* K-Alpha XPS instrument (ESCA) with X-rays generated by a 12 kV electron beam with a spot size of 400 mm. The O/C ratio and peak deconvolution were quantified by *Thermo Scientific Avantage* software, and then converted to mass ratio by using C and O atomic weights. The XPS instrumental error for atomic composition is ±1%, and the accuracy of the C1s peak fitting is ±2%.

Thermogravimetric analysis (TGA). The HCM thermal stability was evaluated with a *Discovery TGA*. The samples were cut into 5 × 5 mm^2 pieces for a total weight of ~5 mg. The target temperature was set to 500 ºC with a 10 ºC/min heating rate under air flow (25 ml^{-1}). The mass change over time was monitored and quantified with *Trios* software.

2.4 Permeability and Rejection Test

The HCM were tested using a multi-cell cross-flow apparatus (see Figure S3 in the SI). The cross-flow apparatus allows the simultaneous evaluation of nine membranes at a pressure ranging from 4 to 10 bar. The effective filtration area for each membrane is 3 x 7 cm^2. The pure water permeability, expressed in LMH-bar, was evaluated by monitoring the permeate volume with a *Sartorious* Laboratory balance every 30 or 60 min.

The permeate was collected in vials and the conductivity rejection was calculated with equation 1:

$$R = \left(1 - \frac{C_p}{C_f}\right) * 100 \qquad \text{(Eq. 1)}$$

where C_p and C_f are the conductivity of the permeate and the feed, respectively.

The conductivity rejection tests were carried out with a 1 mM NaCl and 1 mM Na_2SO_4 aqueous solution. The conductivity rejection was determined with a *Thermo Fisher Scientific*

conductivity probe. Organic dyes are traditionally used to initially test nanofiltration membrane efficacy. However, carbon nanomaterials, such as CNT, are characterized by higher adsorption of organic molecules especially aromatic molecules such as dyes,[35] thus we decided to focus on ion rejection and the physical size exclusion mechanism. The ion rejection experiments presented here will also have more relevance toward AWWT applications where ion rejection is desired. Moreover, the ion hydrated radius is smaller than aromatic molecules, thus are more challenging to reject via size exclusion.

The individual ion rejection (R_{ion}) was calculated with an equation similar to Eq.1:

$$R_{ion} = \left(1 - \frac{C_{ion,p}}{C_{ion,f}}\right) * 100 \quad \text{(Eq. 2)}$$

where $C_{ion,p}$ and $C_{ion,f}$ are the specific ion concentration in the permeate and the feed, respectively. The anion (Cl^- and SO_4^{2-}) concentrations were measured with a Dionex ICS-3000 Ion Chromatograph (Dionex Corporation, Sunnyvale, CA) consisting of a SP single pump, DC detector, AS40 autosampler, and a Chromeleon 6.8 software. Cl^- and SO_4^{2-}were separated from other anions using a Dionex IonPac AS25 analytical column (4.0 x 250 mm^2) and a Dionex IonPac AS25 guard column (4.0 x 50 mm^2) with anion self-regenerating suppressor (ERS 500) in recycle mode. Mobile phase (21 mM NaOH) was prepared using a 50% (w/w) sodium hydroxide aqueous solution and deionized water (18.2 MΩ-cm). The isocratic eluent flow rate was 1 mL min^{-1} for 6 min with an injection volume of 50 µL and a column temperature of 30 ^oC. Quantification of individual ions was done using a five-point linear calibration curve over the range of 5-100 mg/L. All samples were diluted before injection and blanks were included in each run. Standard additions were used to confirm the retention time of each anion.

Theoretical ion rejection can also be calculated using Eq. 3:[36]

$$R_{ion} = 1 - 2\left(1 - \frac{d_{ion}}{d_{pore}}\right)^2 + \left(1 - \frac{d_{ion}}{d_{pore}}\right)^4 \quad \text{(Eq. 3)}$$

where d_{ion} and d_{pore} are the diameter of the hydrated ions and the equivalent pore size based on a cylindrical pore assumption, respectively.

The wet flow curves of the membranes were calculated by the capillary flow porometry (CFP) method using a gas-liquid displacement Porometer (*POROLUX*™ 100, Porometer). CFP is based on the displacement of a wetting liquid inside a porous network by means of an inert gas flow. In this study, *POREFIL*® (Porometer, surface tension γ = 16 dyne/cm) was used as the wetting liquid agent, compressed air was used as the inert gas, and the pressure scan method was applied within a pressure range of 0–5.5 bar at room temperature (~23ºC). The membranes were first wetted by the *POREFIL*® and the gas permeation flow was measured by increasing

the transmembrane pressure at a rate of 0.0125 bar/s to obtain the wet curve. The diameter of all the samples was 18.5 mm. At least three different samples for each membrane were evaluated to obtain the final reported wet flow curve.

2.5 HCM Stability

The chemical stability of the HCM was evaluated by comparing the membrane performance (rejection and permeability) before and after 9 hr of 1000 ppm NaClO filtration at 5 bar of applied pressure. Moreover, the surface chemistry of the HCM exposed to chlorination was compared to that of the control ones (exposed to DI). In terms of thermal stability, the surface chemistry of membranes exposed to multiple annealing cycles (up to four) at 150 °C in air was compared to the chemistry of membranes exposed to a single annealing cycle to evaluate any thermal modifications of the surface. TGA analysis was also performed to observe the loss in HCM mass post-exposure to annealing cycles in air.

3. RESULTS and DISCUSSION

3.1 HCM Characterization

The HCM is characterized by a hierarchical structure composed of three layers: a CF layer, a CNT layer, and a GO layer as displayed in Figure 1. More details about these three layers can also be found in the SEM images displayed in Figure S4. The quantitative morphology dimensions of these carbon nanostructures, summarized in Table 1, were determined via statistical analysis (see Figure S5 in the SI for more detail) of the SEM images in Figures 1 and S4.

Table 1: Specifications of the HCM hierarchical structure.

Layer	Material	Dimensions (SEM)	Elemental Composition (XPS)
1st	Carbon Fiber (CF)	CF Diameter: 6.8±0.5 μm Thickness: 160±10 μm Pore Size*: 41±5 μm	C: 95.5±1.0%, O: 4.5±1.0%
2nd	Carbon Nanotubes (CNT)-Nafion (includes intermediate CNT-GO)	CNT Diameter: 16.5±1.3 nm Thickness: ~10 μm CNT length: 100 μm Pore Size*: 208±60 nm	C: 78±1%, F:19±1%, O:3±1%
3rd	Graphene Oxide (GO)	Thickness: 200-300 nm GO flake area: 10 μm^2	C: 70±1%, O: 30±1% (before reduction)

		GO flake thickness: ~1.5 nm** Pore Size*: Dense layer	C: 82±1%, O: 18±9% (after reduction)

*Superficial pore size measured at the feed side of the membrane.
**Based on reference [37]

The first layer is a commercially available carbon paper, which is a porous (41±5 μm superficial pore size) composed of "graphitized" resin bonded CF. The fibers are circa 6.8±0.5 μm in diameter. The CF paper layer has a low compressibility and is highly permeable (800 LMH-bar) and constitutes the mechanical substrate of the HCM. The second layer is composed of an intercalated multi-walled CNT network with a thickness of ~10 μm. Individual CNT have an average length of 100 μm (manufacturer data) and an average diameter of 16.5±1.3 nm (experimental data), which agrees with the reported value from the manufacturer (15 nm). The CNT layer creates a permeable network (25 LMH-bar) with an average superficial pore size of ~200 nm onto which a GO solution can be vacuum filtered. The GO solution is composed of single-atom-thick GO sheets with an average flake area of 10 μm^2. The micrometer-sized GO flakes are stacked on top of each other creating a 200-300 nm thick selective layer comparable in thickness to the polyamide layer used in thin-film composite (TFC) membranes. The importance of having a nm-thin selective layer is two-fold. First, a thinner membrane requires less driving force (i.e., Darcy's Law) resulting in a more energy-efficient membrane. Second, thin selective layers, which conserve the underlying morphology (see Figure S4), are fundamental in regard to membranes whose performance is enhanced by the underlying microstructure.[34] For instance, this is the case for antifouling membranes in which the surface morphology of the membranes plays a pivotal role.[38]

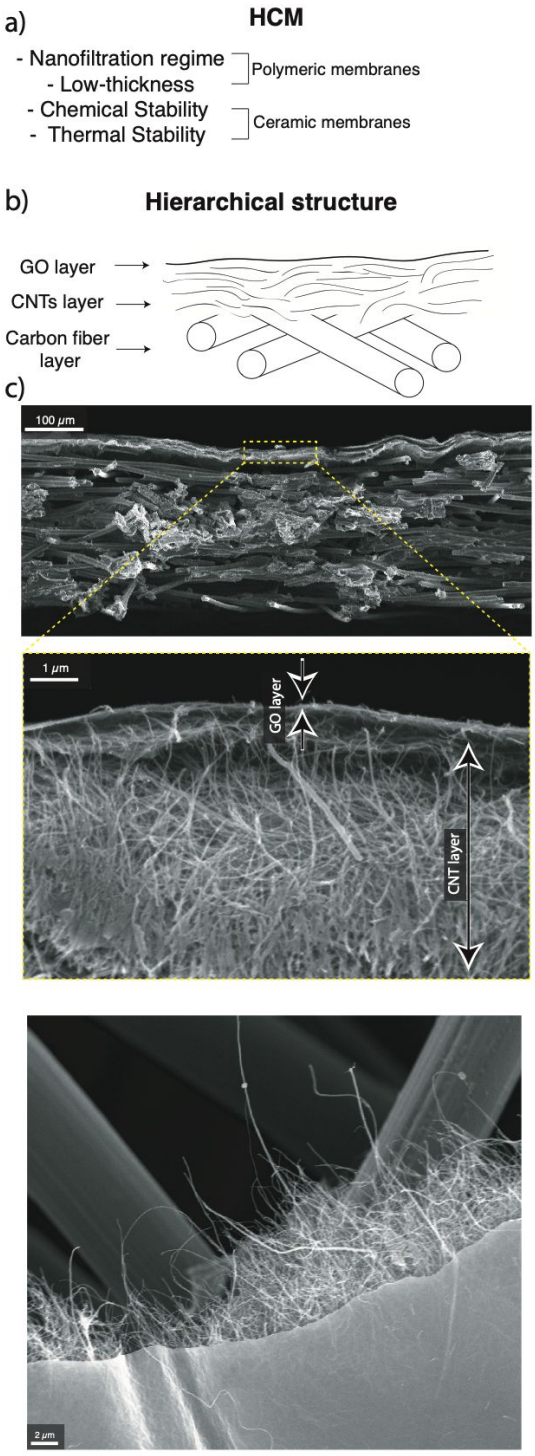

Figure 1: HCM advantages and hierarchical structure. a) Advantages of HCM compared to traditional polymer and ceramic materials. **b)** Schematic of the HCM hierarchical structure composed of three layers (GO, CNT, and CF). **c)** SEM images of a HCM: top image is a cross-section of a HCM, middle image is a zoom-in of the cross-section (the thickness of the CNT and GO layers are identified with arrows) and bottom image is an aerial view of the HCM in which the three carbon architectures (CF, CNT, and GO) are visible.

The HCM support layer could be used in electrochemical processes to degrade small organic molecules that are able to permeate through the GO layer. However, these studies are beyond the current investigation, but reader can consult previous work on the electrochemical response on carbon nanomaterials.

The elemental composition of the HCM is dominated by carbon (>75% atomic C). The CF layer contains the least amount of oxygen due to the graphitization of the fibers during the fabrication process. The CNT layer contains 19% fluorine (F) due to the addition of Nafion to increase CNT dispersion in IPA. The oxygen content of the GO layer significantly decreases from 30 to 18% after the thermal annealing and subsequent chemical reduction of the oxy-functionalities. XPS of the GO layer indicates the hydrophobic Nafion perfluoro-chains do not migrate to the outer GO layer, therefore hydrophobic interactions of these perfluoro-chains will not affect the membrane rejection and transport of ions.

3.2 HCM Permeability and Rejection

HCM permeability was evaluated in a cross-flow apparatus (see Experimental) at pressures ranging from 4 to 10 bar. Application of pressures greater than 10 bar damaged the membranes by creating holes or fractures in the selective layer (see Figure S6 in the SI for an example of mechanically-damaged HCM), resulting in a significant increase in membrane permeability. The majority of the previous GO membrane research was performed in dead-end filtration mode, whereas commercial application of nanofiltration membranes is predominately performed in the cross-flow configuration. Thus, here we challenged the elemental carbon membranes in cross-flow mode as a more practical operational environmental and to reveal differences in physical cross-flow phenomena as compared to dead-end filtration. Similar to polymeric membranes, the HCM experienced compaction and permeability reduction during initial operation likely caused by the pressure-induced changes in the HCM selective GO layer microstructure. The red circles in Figure 2 display the reduction in normalized permeability (to the initial value) over time under 5 bar of applied pressure for two HCM (main plot and inset plot, respectively). The compression/compaction stage required more than 30 hours to achieve steady-state permeability, which was about 10-15% of the initial permeability. Chong et al. recently reported similar behavior for GO membranes with a reduction of nearly 80% of the initial flux due to the compression of GO laminate interlayer spacing.[39] Although the magnitude of the HCM permeability reduction is in agreement with the previous study, more time (approximately 30 hr versus 5 hr) was needed here to reach steady-state permeation. The longer time is likely connected to the presence of void cavities in the HCM structural hierarchy

(CF & CNT) as compared to previous studies in which a GO layer was cast on top of a denser polymeric substrate. The longer compaction time may also be connected to the filtration mode of operation as Chong et al. utilized a 6 bar dead-end filtration in comparison to the 5 bar cross-flow filtration used here.[40] Alternatively, concentration polarization could be the cause of the permeability reduction; however, we ruled out this hypothesis as the CP process would occur on a significantly faster timescale (<1 hr) than observed in our experiments here. [41]

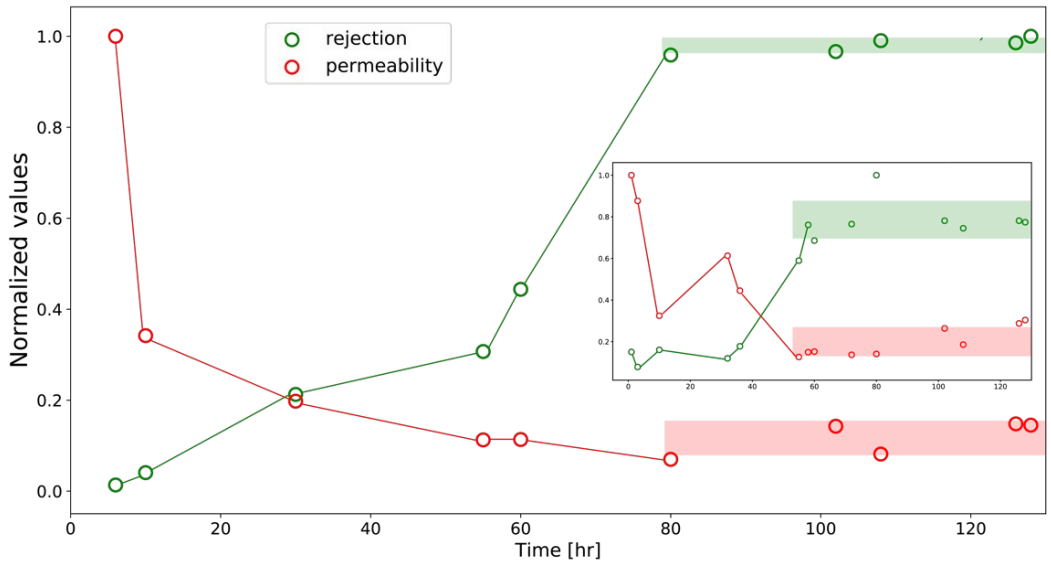

Figure 2. Representative HCM Filtration Permeability and Rejection Performance. Permeability (red circles) and conductivity rejection (green circles) performance over time at 5 bar of applied pressure. The inset represents the performance of a second HCM membrane. The change over time is influenced by the compaction of the HCM hierarchical structure. Steady state values are 1.3 LMH-bar for permeability and 85% for rejection. The shaded regions represent two standard deviations of the average values.

The steady-state permeability of the HCM was 1.3 ± 0.6 LMH-bar, which is in accordance with a previous study and is in the nanofiltration regime.[42] The green circles in Figure 2 represent the normalized conductivity rejection (R) of a solution containing monovalent (Na^+, Cl^-) and polyvalent ions (SO_4^{2-}). As expected the conductivity rejection follows an inverse trend compared to the permeability with rejection increasing during GO selective layer compaction from <10% to ~85%. The permeability and rejection performance of HCM studied here are on the same order of magnitude but lesser than the reported performance of commercial Dow NF270 polyamide membranes (permeability = 5.0 ±0.9 LMH-bar; $SO4^{2-}$ rejection = 92.6±2.1 %). Although the HCM have a slightly lesser

performance than commercial polymeric membranes, the HCM are significantly more resistant to harsh chemical and thermal cleaning treatments. The HCM ions rejection results presented here are in accordance with previous reports on pressure-driven GO selective-layer filtration experiments (Table S1 in the SI). [43-49] Increased ion rejection (e.g. >95%) can be achieved when GO is used in combination with another selective layer such as polyamide and/or polymer cross-linkers; however, these will combinations will have reduced chemical/thermal stability.[27, 50]

The specific ion rejection (R_{ion}) was evaluated via ion chromatography of the feed and permeate (see Experimental). The membranes display a moderate selectivity (36±5%) for monovalent anions such as Cl^-. This is in agreement with studies that highlighted the inefficacy of GO membranes to sieve monovalent ions.[26],[49] However, we observe a greater selectivity ($86 \pm 4\%$) for multivalent ions such as sulfate. The diameter of the membrane pores (d_{pore}) can be estimated using Eq. 3 in the experimental section, which describes a physical size exclusion mechanism. For example, using the rejection values obtained for Cl^- and SO_4^{2-} (~36% and ~86%) and their corresponding hydrated diameters (0.66 and 0.76 nm), an average d_{pore} of 1.83 and 1.05 nm, respectively, was estimated for the membranes. The discrepancy in the pore size dimension here is related to charge repulsion effects connected to the divalency of the sulfate anion, which increases rejection leading to smaller 'effective' pore sizes estimated by Eq. 3.

For GO membranes, the physical pore size or 'diameter' is related to the interlayer distance (*2d*) between GO flakes, which can be estimated from X-ray diffraction measurements. Previous X-ray diffraction studies indicate a *2d* value around 0.8 nm for a dry GO membrane.[42],[51],[52] Under aqueous operation, the membrane will be hydrated and the GO laminate will undergo swelling characterized by a factor around 2, thus leading to a hydrated GO interlayer distance (*2d*) between 1.5 and 2 nm.[53],[54],[55] This value range is in agreement with the d_{pore} value estimated using chlorine rejection (i.e. 1.83 nm) and is also consistent with the results obtained in previous reports.[56]

3.3 HCM Chemical Stability

The HCM chemical stability was initially evaluated using the common oxidant sodium hypochlorite (NaClO). Anion (Cl^-, SO_4^{2-}) rejection before and after filtering 1000 ppm NaClO through the HCM for 9 hours at 5 bar is displayed in Figure 3a. Chlorination did not have a significant effect on HCM anion rejection highlighting the HCM chemical resistance to oxidizing agents. The slight increase in observed HCM anion rejection suggests a decrease of

the GO interlayer spacing as a result of NaClO addition, which increases the feed pH to 10 and reduces the ionic GO interlayer screening effect resulting in narrower GO channels/pore size.[57] This increase in anion rejection is also supported by the results obtained from CFP measurements, as shown in Figure 3b and Figure S7. The chlorination process decreases the membranes wet flow by a factor of 5 at approximately 4 bar. The decrease and the absolute value of flow rate here cannot be directly compared to the value obtained with the saline solutions as the CFP analysis is carried out with a very low surface tension wetting liquid (POREFIL®, 16 dyne/cm) as compared to that of water (72 dyne/cm). Moreover, the driving force behind the CFP is capillary, which is different as compared to the pressurized aqueous flow used in the cross-flow setup. In summary, the analyses completed here exemplify the HCM chemical stability and their resilience to oxidizing cleaning solutions since the extended permeation of concentrated NaClO did not have a significant negative effect on the HCM permeability and rejection.

To further evaluate the HCM stability to oxidants, their surface chemistry was characterized via XPS as displayed in Figure 3c. The untreated and chlorinated HCM are characterized by an XPS O/C ratio of 0.38 and 0.43, respectively, revealing minor surface oxidation post-chlorination. Even though the membranes were rinsed with copious DI water post-chlorination, the chlorinated HCM XPS is influenced by the presence of surface-associated ions, e.g. 2% Na in HCM atomic composition. The slightly increased O/C content of the chlorinated HCM can also be observed in the deconvolution of the C1s high resolution spectra, which is characterized by three peaks corresponding to: (i) single (C–C) and double (C=C) carbon bonds centered at 285 eV; (ii) epoxide (C–O–C) and hydroxide (C–OH) functional groups centered at 287 eV; and (iii) carboxylate (O=C–OH) functional groups centered at 289 eV. In particular, HCM chlorination results in a 4-5% increase in the epoxide concentration, followed by the same magnitude decrease of the carbon sp^2 signal centered at 285 eV. Thermal annealing in an inert atmosphere would reduce the formed epoxides back to olefins returning the membranes to their original state.

HCM chemical stability was also challenged with common organic solvents such as acetone. The immersion of NF270 membranes in acetone quickly and permanently degrades the thin film composite membrane (see video in the SI) with the selective and ultrafiltration layers detaching from the substrate and semi-dissolving into an unusable crumpled mass.. In stark contrast, the HCM are resistant to organic solvent degradation (see video in the SI). The HCM organic solvent stability can be also verified by examining surficial SEM images

presented in Figure S8, which reveals similar morphology (i.e. no visible damage) for HCM immersed in acetone compared to that of HCM immersed in water. For example, after acetone immersion, the GO and CNT layers still homogeneously cover the underlying CF paper, preserving its morphology as single carbon fibers are still recognizable. This experiment highlights the stability of the HCM structure, but further permeability experiments might be required to corroborate the ability to HCM to still operate in the NF regime after solvent exposure. Stability to organic solvents may open new avenues for membrane cleaning e.g. a carbon nanotube electrochemical filter poisoned with an insulating polymer coating could be regenerated using an organic solvent.[58] Moreover, organic solvent resistance opens the HCM to a range of separation applications such as those in the petrochemical, food processing, and pharmaceutical industries, which commonly involve the use of aggressive aprotic solvents (e.g. acetone).[59]

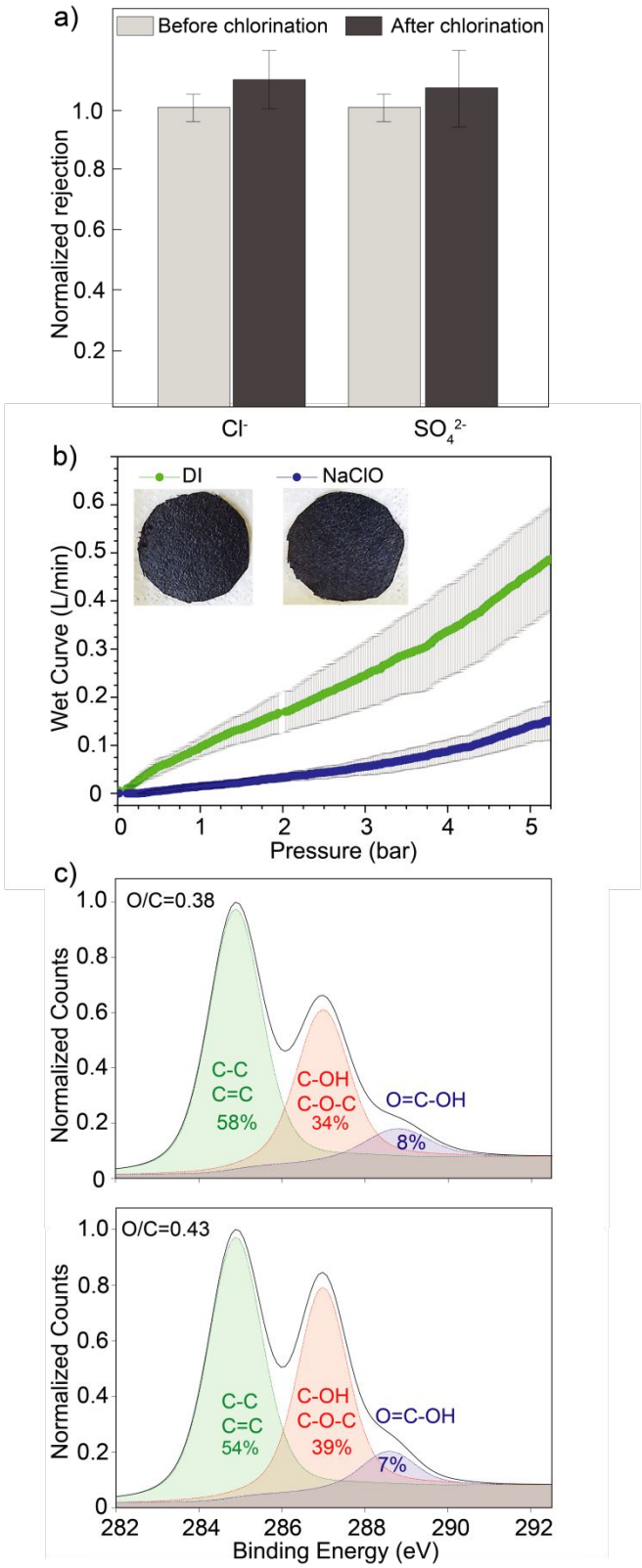

Figure 3: HCM Chemical Stability. a) Normalized ions rejection before (light grey) and after (dark grey) chlorination. **The normalization value is 86% for SO_4^{2-} and 36% for Cl^- and data refer to the average of six membranes tested. b)** CFP analysis of HCM after DI filtration (in green) and NaClO filtration (in blue). The figure includes photos of the HCM used in the analysis. **c)** C1s deconvolution spectra of the HCM before (top) and after (bottom) chlorination.

3.4 HCM Thermal Stability

HCM thermal stability was initially evaluated during the fabrication process where the HCM were reduced at 150 °C in a nitrogen atmosphere. No physical damage was observed to either the selective layer or the underlying substrate after this thermal annealing process. The fact that membrane can reject ions after this thermal annealing indicates that the membranes are resistant to the thermal pretreatment. The results of previous studies highlight the thermal stability of CNT and CF paper up to 300-400 °C [60] in air; and once reduced, GO tends to be stable under similar thermal conditions. More intense GO thermal treatment (e.g. T >350 °C) will lead to thermolysis of oxygen functionalities and possibly defect formation in the parent sp^2 graphene sheet.[61] However, the results presented here highlight a material improvement as compared to previous studies in which the elemental carbon nanomaterials were cast onto a polymeric membrane substrate (e.g. PVDF), which would prevent thermal heating above 100 °C. Moreover, the thermal treatment completely degraded the NF270 physical structure resulting in a unworkable mass, as expected. To corroborate the HCM thermal stability, the membranes were subjected to four sequential thermal annealing cycles of 15 min at 150 °C in an oxidizing environment (i.e. ambient air). Afterwards, the XPS C1s peak profiles of the HCM (see Figure 4 and Table S2 in the SI) were used to evaluate the effect of the annealing cycles on the HCM surface chemistry. The sp^2 peak (C-C; C=C) is constant at ~65% before and after every annealing cycle highlighting the HCM thermal stability. A TGA (Figure S9 in the SI) indicates that the HCM is stable until 350 °C with less than 0.1% loss in mass; at this temperature, the $\Delta m/\Delta T$ begins to increase signaling the onset of HCM thermal decomposition. For comparison, a traditional polyamide TFC is observed to lose 70% of its mass by 500 °C, whereas the loss is <1% for an HCM. The HCM thermal stability can be utilized for membrane regeneration similar to ceramic membranes, in which the regeneration temperature (>200 °C) depends on the adsorbed/deposited species.[62] This latter property could increase the reuse of the membrane and its life span. The superior HCM thermal stability compared to traditional polymeric membranes will increase potential for a broader range of industrial applications such as the treatment of cooling/boiler water in thermoelectric generation plants or oil/water separations in petroleum processing plants.

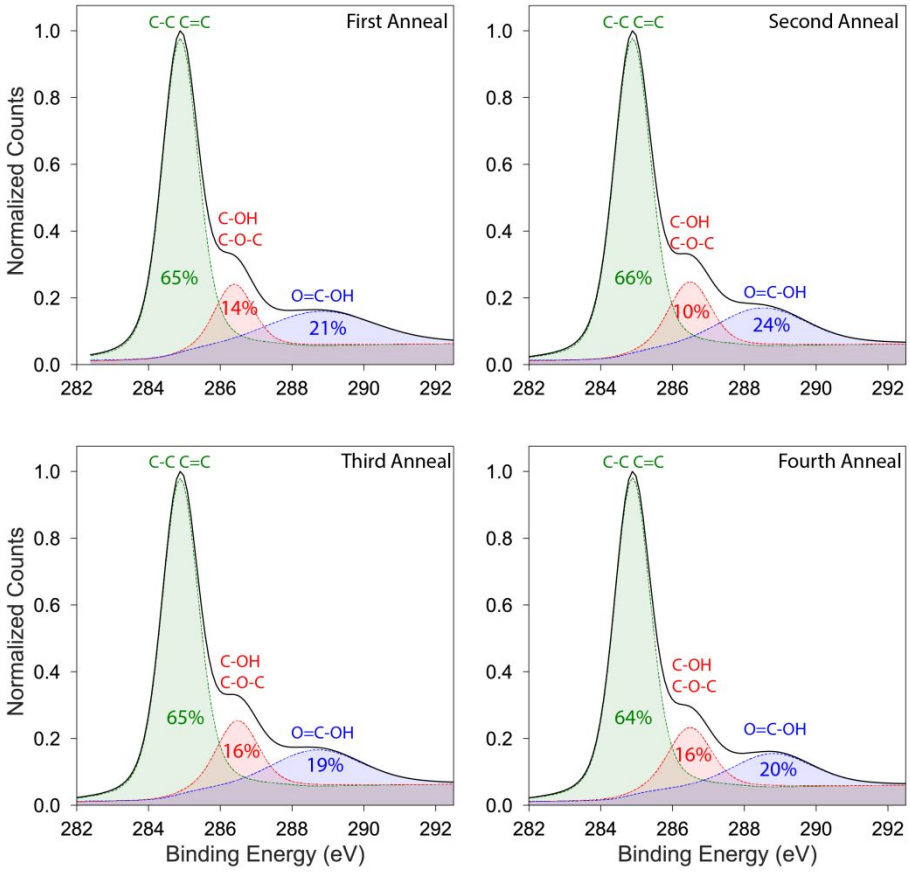

Figure 4: HCM thermal stability. C1s deconvolution spectra of the HCM subjected to four annealing cycles of 15 min at 150 °C in an oxidizing environment (i.e. ambient air).

3.5 Non-Linear and Reversible HCM Permeability Pressure-Dependence

Here, the HCM pressure-dependent permeability post-compaction was investigated as displayed in Figure 5. Of note is that when the applied pressure is increased from 4.5 to 7.5 bar (1.67-fold) the normalized permeability (in red) increases from 0.4 to 0.9 (2.25-fold), which is at odds with Darcy's Law that predicts a pressure-independent permeability. This behavior has been previously reported both experimentally and through molecular dynamic simulations for carbon nanostructures [63],[64] and it differs from polymeric membranes behavior, where the pressure-normalized flux (i.e. LMH-bar) is invariant of the applied pressure. The increase in permeability with increasing pressure is corroborated by a concomitant decrease in ion rejection of around 1.6-fold (in green). The decrease in the rejection at higher

pressures may be related to the energy barrier required to dehydrate ions since similar barrier is also present in the disruption of the hydrogen bond network for water entering in the GO nanochannels from the bulk. However, the latter energy is significantly lower than the necessary dehydration of ions (≈6 kJ/mol versus 10^2-10^3 kJ/mol); in other words, the low pressure increase (~ 3 bar) provides enough energy to break the hydrogen bonding network, but is not sufficient for the dehydration of the ions.[65] Thus, pressure-induced ion dehydration is likely not active here.

Thus at first glance, the decrease in the rejection could also be attributed to pressure-induced membrane damage. However, once the pressure is returned from 7.5 to 4.5 bar, both the HCM permeability and rejection reversibly return to their original state and this phenomenon was reproduced with a number of HCM samples (see Figure S10 in the SI). The reversibility of HCM performance with pressure could be a noteworthy addition to the recent developments in the field of active membranes. In particular, there is a continuous effort to develop smart membranes that are active and/or reactive in response to external stimuli. For example, a recent study demonstrated that GO membrane performance can be altered by an externally applied unidirectional force.[66] GO studies have also used other externally applied stimuli such as voltage, which ionizes water molecules inside the GO channel leading to a blockage of water transport.[67] Similarly, studies have attempted to modify the structure of the GO nanochannel by altering the pH of the feed, inducing pH-dependent membrane performance phenomena.[45] Thus, the ability of the GO nanostructure to adapt to multiple external stimuli makes it an ideal candidate for the fabrication of structurally-active membranes with reversible behavior.

Note, that for structurally-active membranes the traditional water transport model (i.e. Darcy's) will not hold as the applied pressure may alter the structure of the membrane such as the spatial arrangement of the GO oxy-functionalities.[68] One hypothesis for the increased permeability and decreased rejection at higher pressure can be connected to the pressure-induced desorption of water molecules from the GO walls and oxy-functional groups.[69] In this scenario, the desorption of water molecules from the GO nanochannel inner walls yields a larger effective channel width (i.e., effective 'pore' size) and thus higher permeability and lower rejection.

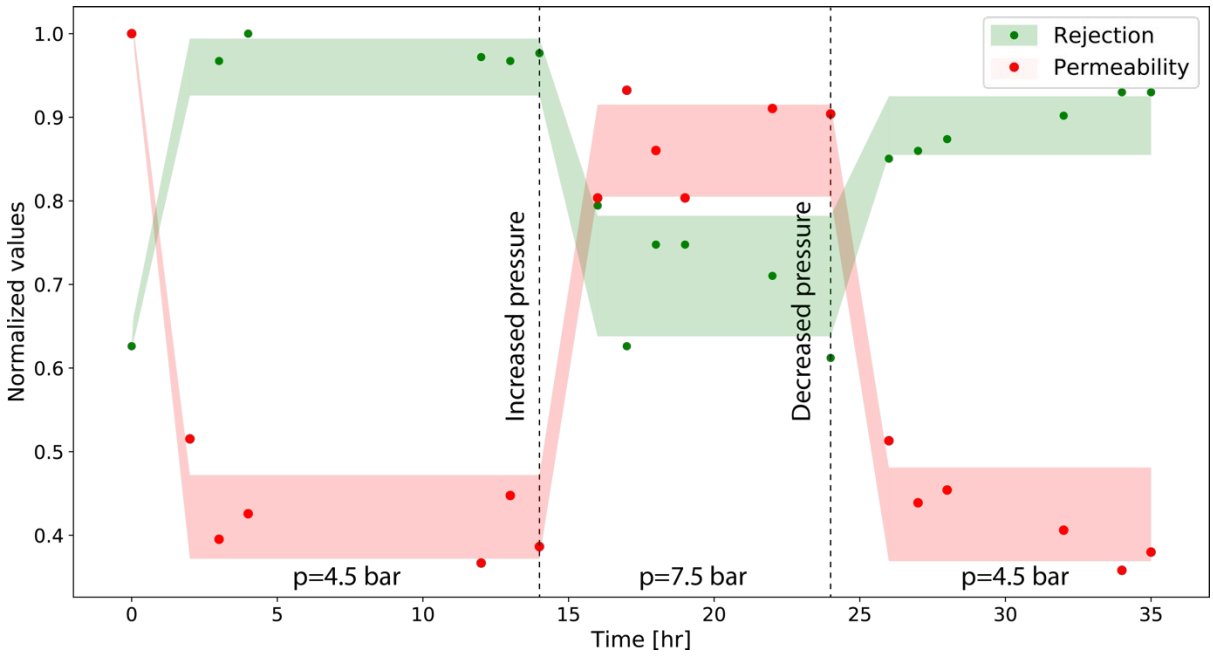

Figure 5:.Representative HCM Reversible Pressure-Induced Behavior. Permeability (red circles) and rejection (green circles) performance of a HCM over time under different pressures applied (7.5 and 4.5 bar). The shaded regions represent two standard deviations of the average values. The dashed line indicates the times when the pressure was changed.

4. CONCLUSIONS

This investigation highlights the possibility of creating an elemental carbon-based hierarchal membrane that possesses the combined advantages of typically disparate polymeric and ceramic membranes. The unique HCM characteristics are a result of the layer-by-layer nano-manipulation of the elemental carbon architectures embedded in its hierarchical structure. The HCM operates in the nanofiltration regime similar to polymeric and, concurrently display the chemical and thermal stability typical of ceramic membranes. Specifically, HCM have a nanoscale pore size (<2 nm), which effectively reject polyvalent ions, and are also resistant to chlorine oxidants, high pH, organic solvents, and elevated temperatures (>150 °C). The investigation also displayed the ability to use externally applied pressure as a potential stimulus to control performance in-situ, highlighting the structurally-active and reversible behavior of the HCM. Through this initial HCM development we hope to spark a new direction of research in membrane materials displaying polymer-ceramic hybrid properties, cultivating new material ideas, promoting membrane progress, supporting continued AWWT efforts, and thus ultimately contributing to the increase of global water resources.

ACKNOWLEDGMENTS

US Bureau of Reclamation's (USBR) Water Quality Improvement Center (WQIC), AMTA fellowship, and by the Korea Institute of Geoscience and Mineral Resources. This work made use of the Center for Nanoscale Systems at Harvard University, a member of the National Nanotechnology Infrastructure Network, supported (in part) by the National Science Foundation under NSF award number ECS-0335765. The authors would like to thank the USBR's WQIC for the technical support and equipment provided on an in-kind services basis. TGA analysis were carried out at Wyss Institute facilities at Harvard under the supervision of Jack Alvarenga. The authors would also like to thank Harvard John A. Paulson SEAS course ES91r which allowed undergraduate students Daniel Chang, Cailey Martin, Leticia Ortega, and Jazmin Simpkins to participate in this research.

REFERENCES

1. K.P. Loh, Q. Bao, G. Eda, and M. Chhowalla; Graphene oxide as a chemically tunable platform for optical applications. *Nat. Chem.* **2010**, *2*, 1015;
2. R.H. Tunuguntla, R.Y. Henley, Y.-C. Yao, T.A. Pham, M. Wanunu, and A. Noy; Enhanced water permeability and tunable ion selectivity in subnanometer carbon nanotube porins. *Science*. **2017**, *357*, 792-796;
3. K.S. Novoselov, A.K. Geim, S.V. Morozov, D. Jiang, Y. Zhang, S.V. Dubonos, I.V. Grigorieva, and A.A. Firsov; Electric field effect in atomically thin carbon films. *Science*. **2004**, *306*, 666-669;
4. F. Li, X. Jiang, J. Zhao, and S. Zhang; Graphene oxide: A promising nanomaterial for energy and environmental applications. *Nano energy*. **2015**, *16*, 488-515;
5. S.Y. Lim, W. Shen, and Z. Gao; Carbon quantum dots and their applications. *Chem. Soc. Rev.* **2015**, *44*, 362-381;
6. S. Kumar, R. Rani, N. Dilbaghi, K. Tankeshwar, and K.-H. Kim; Carbon nanotubes: a novel material for multifaceted applications in human healthcare. *Chem. Soc. Rev.* **2017**, *46*, 158-196;
7. X. Zhu, K. Yang, and B. Chen; Membranes prepared from graphene-based nanomaterials for sustainable applications: a review. *Environmental Science: Nano*. **2017**, *4*, 2267-2285;
8. Y. Shen, Q. Fang, and B. Chen; Environmental applications of three-dimensional graphene-based macrostructures: adsorption, transformation, and detection. *Environ. Sci. Technol.* **2014**, *49*, 67-84;
9. J. Lee, I.Y. Stein, S.S. Kessler, and B.L. Wardle; Aligned carbon nanotube film enables thermally induced state transformations in layered polymeric materials. *ACS Appl. Mater. Interfaces*. **2015**, *7*, 8900-8905;
10. K. Yang, J. Wang, X. Chen, Q. Zhao, A. Ghaffar, and B. Chen; Application of graphene-based materials in water purification: from the nanoscale to specific devices. *Environmental Science: Nano*. **2018**, *5*, 1264-1297;
11. M. Li, C. Wang, M.J. O'Connell, and C.K. Chan; Carbon nanosphere adsorbents for removal of arsenate and selenate from water. *Environmental Science: Nano*. **2015**, *2*, 245-250;
12. G. Ferrero, M.S. Bock, E.H. Stenby, C. Hou, and J. Zhang; Reduced Graphene Oxide-Coated Microfibers for Oil-Water Separation. *Environmental Science: Nano*. **2019**;
13. Q. Wang, C. Aubry, Y. Chen, H. Song, and L. Zou; Insights on tuning the nanostructure of rGO laminate membranes for low pressure osmosis process. *ACS Appl. Mater. Interfaces*. **2017**, *9*, 22509-22517;
14. K.S. Novoselov, V.I. Falko, L. Colombo, P.R. Gellert, M.G. Schwab, and K. Kim; A roadmap for graphene. *Nature*. **2012**, *490*, 192-200;
15. G.-P. Hao, W.-C. Li, and A.-H. Lu; Novel porous solids for carbon dioxide capture. *J. Mater. Chem.* **2011**, *21*, 6447-6451;
16. M. Ebrahimi, D. Willershausen, K.S. Ashaghi, L. Engel, L. Placido, P. Mund, P. Bolduan, and P. Czermak; Investigations on the use of different ceramic membranes for efficient oil-field produced water treatment. *Desalination*. **2010**, *250*, 991-996;
17. R. Baker, *Membrane Technology and Applications* 2012.
18. W.J. Koros, Y.H. Ma, and T. Shimidzu, *Terminology for membranes and membrane processes (IUPAC Recommendations 1996)*, in *Pure Appl. Chem.* 1996. p. 1479.

19. M. Safarpour, A. Khataee, and V. Vatanpour; Thin film nanocomposite reverse osmosis membrane modified by reduced graphene oxide/TiO2 with improved desalination performance. *J. Membr. Sci.* **2015**, *489*, 43-54;
20. S.H. Dave, B.D. Keller, K. Golmer, and J.C. Grossman; Six Degrees of Separation: Connecting Research with Users and Cost Analysis. *Joule*. **2017**, *1*, 410-415;
21. H.-R. Chae, J. Lee, C.-H. Lee, I.-C. Kim, and P.-K. Park; Graphene oxide-embedded thin-film composite reverse osmosis membrane with high flux, anti-biofouling, and chlorine resistance. *J. Membr. Sci.* **2015**, *483*, 128-135;
22. K. Goh, W. Jiang, H.E. Karahan, S. Zhai, L. Wei, D. Yu, A.G. Fane, R. Wang, and Y. Chen; All-Carbon Nanoarchitectures as High-Performance Separation Membranes with Superior Stability. *Adv. Funct. Mater.* **2015**, *25*, 7348-7359;
23. C.A. Amadei and C.D. Vecitis; How to Increase the Signal-to-Noise Ratio of Graphene Oxide Membrane Research. *J. Phys. Chem. Lett.* **2016**, *7*, 3791-3797;
24. S. Xia, M. Ni, T. Zhu, Y. Zhao, and N. Li; Ultrathin graphene oxide nanosheet membranes with various d-spacing assembled using the pressure-assisted filtration method for removing natural organic matter. *Desalination*. **2015**, *371*, 78-87;
25. L. Huang, J. Chen, T. Gao, M. Zhang, Y. Li, L. Dai, L. Qu, and G. Shi; Reduced graphene oxide membranes for ultrafast organic solvent nanofiltration. *Adv. Mater.* **2016**, *28*, 8669-8674;
26. L. Chen, et al.; Ion sieving in graphene oxide membranes via cationic control of interlayer spacing. *Nature*. **2017**, *550*, 380;
27. Y. Qian, C. Zhou, and A. Huang; Cross-linking modification with diamine monomers to enhance desalination performance of graphene oxide membranes. *Carbon*. **2018**, *136*, 28-37;
28. C.-N. Yeh, K. Raidongia, J. Shao, Q.-H. Yang, and J. Huang; On the origin of the stability of graphene oxide membranes in water. *Nat. Chem.* **2015**, *7*, 166-170;
29. X. Ma, R. Swaidan, B. Teng, H. Tan, O. Salinas, E. Litwiller, Y. Han, and I. Pinnau; Carbon molecular sieve gas separation membranes based on an intrinsically microporous polyimide precursor. *Carbon*. **2013**, *62*, 88-96;
30. J.S. Adams, A.K. Itta, C. Zhang, G.B. Wenz, O. Sanyal, and W.J. Koros; New insights into structural evolution in carbon molecular sieve membranes during pyrolysis. *Carbon*. **2019**, *141*, 238-246;
31. S.J. Kim, D.W. Kim, K.M. Cho, K.M. Kang, J. Choi, D. Kim, and H.-T. Jung; Ultrathin graphene oxide membranes on freestanding carbon nanotube supports for enhanced selective permeation in organic solvents. *Scientific Reports*. **2018**, *8*, 1959;
32. W. Peng, H. Li, Y. Liu, and S. Song; Adsorption of methylene blue on graphene oxide prepared from amorphous graphite: Effects of pH and foreign ions. *J. Mol. Liq.* **2016**, *221*, 82-87;
33. Q. Zhang and C.D. Vecitis; Conductive CNT-PVDF membrane for capacitive organic fouling reduction. *J. Membr. Sci.* **2014**, *459*, 143-156;
34. B. Tang, L. Zhang, R. Li, J. Wu, M.N. Hedhili, and P. Wang; Are vacuum-filtrated reduced graphene oxide membranes symmetric? *Nanoscale*. **2016**, *8*, 1108-1116;
35. Y. Li, et al.; Comparative study of methylene blue dye adsorption onto activated carbon, graphene oxide, and carbon nanotubes. *Chem. Eng. Res. Des.* **2013**, *91*, 361-368;
36. M.L. Davis, *Water and Wastewater Engineering*. 2010: Mc-Graw-Hill

.

37. C.A. Amadei, I.Y. Stein, G.J. Silverberg, B.L. Wardle, and C.D. Vecitis; Fabrication and morphology tuning of graphene oxide nanoscrolls. *Nanoscale*. **2016**, *8*, 6783-6791;
38. S. Dervin, D.D. Dionysiou, and S.C. Pillai; 2D nanostructures for water purification: graphene and beyond. *Nanoscale*. **2016**, *8*, 15115-15131;
39. J.Y. Chong, B. Wang, C. Mattevi, and K. Li; Dynamic microstructure of graphene oxide membranes and the permeation flux. *J. Membr. Sci.* **2018**, *549*, 385-392;
40. J.Y. Chong, B. Wang, and K. Li; Water transport through graphene oxide membranes: the roles of driving forces. *Chemical Communications*. **2018**, *54*, 2554-2557;
41. G.A. Xianhui Li, Jiebin Lin, Jianxin Li; Monitoring of Membrane Scaling and Concentration Polarization in Spiral-Wound Reverse Osmosis Module Using Ultrasonic Time-Domain Reflectometry with Sound Intensity Calculation. *Journal of Water Sustainability*. **2014**, *4*, 167-180;
42. C.A. Amadei, A. Montessori, J.P. Kadow, S. Succi, and C.D. Vecitis; Role of Oxygen Functionalities in Graphene Oxide Architectural Laminate Subnanometer Spacing and Water Transport. *Environmental Science & Technology*. **2017**, *51*, 4280-4288;
43. W.L. Xu, C. Fang, F. Zhou, Z. Song, Q. Liu, R. Qiao, and M. Yu; Self-assembly: a facile way of forming ultrathin, high-performance graphene oxide membranes for water purification. *Nano Lett.* **2017**, *17*, 2928-2933;
44. M. Hu and B. Mi; Enabling Graphene Oxide Nanosheets as Water Separation Membranes. *Environ. Sci. Technol.* **2013**, *47*, 3715-3723;
45. Y. Oh, D.L. Armstrong, C. Finnerty, S. Zheng, M. Hu, A. Torrents, and B. Mi; Understanding the pH-responsive behavior of graphene oxide membrane in removing ions and organic micropollulants. *J. Membr. Sci.* **2017**, *541*, 235-243;
46. L. Chen, et al.; High performance graphene oxide nanofiltration membrane prepared by electrospraying for wastewater purification. *Carbon*. **2018**, *130*, 487-494;
47. L. Chen, et al.; A large-area free-standing graphene oxide multilayer membrane with high stability for nanofiltration applications. *Chem. Eng. J.* **2018**, *345*, 536-544;
48. J.-L. Han, et al.; Functional graphene oxide membrane preparation for organics/inorganic salts mixture separation aiming at advanced treatment of refractory wastewater. *Sci. Total Environ.* **2018**, *628*, 261-270;
49. F. Baskoro, C.-B. Wong, S.R. Kumar, C.-W. Chang, C.-H. Chen, D.W. Chen, and S.J. Lue; Graphene oxide-cation interaction: Inter-layer spacing and zeta potential changes in response to various salt solutions. *J. Membr. Sci.* **2018**, *554*, 253-263;
50. G. Lai, W. Lau, P. Goh, A. Ismail, N. Yusof, and Y. Tan; Graphene oxide incorporated thin film nanocomposite nanofiltration membrane for enhanced salt removal performance. *Desalination*. **2016**, *387*, 14-24;
51. B. Qi, X. He, G. Zeng, Y. Pan, G. Li, G. Liu, Y. Zhang, W. Chen, and Y. Sun; Strict molecular sieving over electrodeposited 2D-interspacing-narrowed graphene oxide membranes. *Nature Communications*. **2017**, *8*, 825;
52. W.-S. Hung, C.-H. Tsou, M. De Guzman, Q.-F. An, Y.-L. Liu, Y.-M. Zhang, C.-C. Hu, K.-R. Lee, and J.-Y. Lai; Cross-Linking with Diamine Monomers To Prepare Composite Graphene Oxide-Framework Membranes with Varying d-Spacing. *Chem. Mater.* **2014**, *26*, 2983-2990;
53. K.H. Thebo, X. Qian, Q. Zhang, L. Chen, H.-M. Cheng, and W. Ren; Highly stable graphene-oxide-based membranes with superior permeability. *Nature Communications*. **2018**, *9*, 1486;

54. A.V. Talyzin, T. Hausmaninger, S. You, and T. Szabó; The structure of graphene oxide membranes in liquid water, ethanol and water–ethanol mixtures. *Nanoscale*. **2014**, *6*, 272-281;
55. Q. Yang, et al.; Ultrathin graphene-based membrane with precise molecular sieving and ultrafast solvent permeation. *Nat. Mater.* **2017**, *16*, 1198;
56. J. Abraham, et al.; Tunable sieving of ions using graphene oxide membranes. *Nature nanotechnology*. **2017**, *12*, 546;
57. H. Huang, Y. Mao, Y. Ying, Y. Liu, L. Sun, and X. Peng; Salt concentration, pH and pressure controlled separation of small molecules through lamellar graphene oxide membranes. *Chem. Commun.* **2013**, *49*, 5963-5965;
58. G. Gao and C.D. Vecitis; Electrocatalysis aqueous phenol with carbon nanotubes networks as anodes: Electrodes passivation and regeneration and prevention. *Electrochimica Acta*. **2013**, *98*, 131-138;
59. S. Chisca, P.H.H. Duong, A.H. Emwas, R. Sougrat, and S.P. Nunes; Crosslinked copolyazoles with a zwitterionic structure for organic solvent resistant membranes. *Polymer Chemistry*. **2015**, *6*, 543-554;
60. N. Hordy, D. Rabilloud, J.-L. Meunier, and S. Coulombe; High temperature and long-term stability of carbon nanotube nanofluids for direct absorption solar thermal collectors. *Solar Energy*. **2014**, *105*, 82-90;
61. A. Bagri, C. Mattevi, M. Acik, Y.J. Chabal, M. Chhowalla, and V.B. Shenoy; Structural evolution during the reduction of chemically derived graphene oxide. *Nat. Chem.* **2010**, *2*, 581;
62. A. Dafinov, R. Garcia-Valls, and J. Font; Modification of ceramic membranes by alcohol adsorption. *J. Membr. Sci.* **2002**, *196*, 69-77;
63. L. Liu, X. Xie, R. Zambare, A. Selvaraj, B. Sowrirajalu, X. Song, C. Tang, and C. Gao; Functionalized Graphene Oxide Modified Polyethersulfone Membranes for Low-Pressure Anionic Dye/Salt Fractionation. *Polymers*. **2018**, *10*, 795;
64. A. Nicolaï, B.G. Sumpter, and V. Meunier; Tunable water desalination across graphene oxide framework membranes. *PCCP*. **2014**, *16*, 8646-8654;
65. M. Thomas and B. Corry; A computational assessment of the permeability and salt rejection of carbon nanotube membranes and their application to water desalination. *Philosophical transactions. Series A, Mathematical, physical, and engineering sciences*. **2016**, *374*, 20150020;
66. W. Li, W. Wu, and Z. Li; Controlling interlayer spacing of graphene oxide membranes by external pressure regulation. *ACS nano*. **2018**, *12*, 9309-9317;
67. K.G. Zhou, et al.; Electrically controlled water permeation through graphene oxide membranes. *Nature*. **2018**, *559*, 236-240;
68. C. Fang, X. Wu, F. Yang, and R. Qiao; Flow of quasi-two dimensional water in graphene channels. *J. Chem. Phys.* **2018**, *148*, 064702;
69. B. Chen, H. Jiang, X. Liu, and X. Hu; Water transport confined in graphene oxide channels through the rarefied effect. *PCCP*. **2018**, *20*, 9780-9786;

HIERARCHICAL CARBON MEMBRANE